Joseph M. Kahn
August 23, 2013

Performance Evaluation of ACO-OFDM in Multimode Fiber

This report summarizes a performance evaluation of asymmetrically clipped orthogonal frequency-division multiplexing (ACO-OFDM), an intensity modulation/direct detection format that is promising for very high-speed transmission in multimode fiber (MMF).

Preliminaries

Simplifying Assumptions

The following is a list of assumptions made to simplify the analysis. In addition, several approximations are made, as described in the analysis below.

- We assume the number of subcarriers is large enough that the OFDM signal is Gaussian-distributed.
- We include quantization noise in the A/D converter at the receiver. We neglect quantization effects in the D/A converter at the transmitter, as well as finite-word-length effects in the DSP units at the transmitter and receiver.
- We assume the VCSEL has a linear modulation response up to a power at which clipping occurs. We neglect chirp, intensity noise, and modal noise.
- We neglect chromatic dispersion in the multimode fiber, which allows us to model the intensity response of the fiber as a linear system.
- We assume the receiver noise is additive, signal-independent thermal noise, neglecting shot noise.

Notation

Symbol	Description	Units
N	FFT length	samples
K	Number of positive-frequency data-bearing subcarriers, $1 \le K \le N/4$	–
L	Channel impulse response duration	samples
$L-1$	Cyclic prefix length	samples
T	OFDM symbol duration	s
$R_s = \frac{N}{T}$	Sampling rate	Hz
$r_{os} = \frac{N}{4K}$	Oversampling rate, $1 \le r_{os} \le \frac{N}{4}$	–
$\Delta f = \frac{1}{T} = \frac{R_s}{N+L-1}$	Subcarrier spacing	Hz
$0 \le n \le \frac{N}{2}-1$ $\frac{N}{2} \le n \le N-1$	Indices of $\frac{N}{2}$ positive-frequency subcarriers Indices of $\frac{N}{2}$ negative-frequency subcarriers	–
$1 \le n \le 2K-1$, n odd $n = 2m-1$, $1 \le m \le K$	Indices of K data-bearing positive-frequency subcarriers	–
$f_n = n\Delta f$	Frequencies of $\frac{N}{2}$ positive-frequency subcarriers	Hz

$f_n = (n-N)\Delta f$	Frequencies of $\frac{N}{2}$ negative-frequency subcarriers	
$X_n : \begin{cases} \neq 0 & n \text{ odd} \\ = 0 & n \text{ even} \end{cases}$	Amplitude of *n*th data-bearing electrical subcarrier before clipping (complex)	A
$X_{N-n} = X_n^*$	Hermitean symmetry to ensure real waveform	A
$P_n = E\left(\lvert X_n \rvert^2\right)$	Electrical power of *n*th data-bearing electrical subcarrier	A^2
$x(t)$	Electrical OFDM waveform before clipping (real, bipolar)	A
$x_+(t)$	Electrical OFDM waveform after clipping (real, nonnegative)	A
$E\left(\lvert x(t) \rvert^2\right) = \sigma^2$	Power of electrical OFDM waveform before clipping	A^2
$E\left(\lvert x_+(t) \rvert^2\right) = \frac{\sigma^2}{2}$	Power of electrical OFDM waveform after clipping	A^2
$E\left(\lvert x_+(t) \rvert\right) = \frac{\sigma}{\sqrt{2\pi}}$	Average value of electrical OFDM waveform after clipping	A
$H_l(f)$	VCSEL intensity modulation electrical transfer function, normalized to unity at d.c.	A/A or W/W
κ	VCSEL slope efficiency	W/A
R_l	VCSEL series resistance	Ω
$P(t)$	VCSEL optical intensity waveform (real, nonnegative)	W
P_{avg}	VCSEL optical average power	W
P_{clip}	VCSEL optical power clipping level	W
P_{diss}	VCSEL electrical dissipation average power	W
$H_f(f)$	MMF intensity modulation transfer function scaled so d.c. value corresponds to square of optical transmission coefficient.	A/A or W/W
R	Photodetector responsivity	A/W
$i(t)$	Photocurrent waveform without noise (real, nonnegative)	A
$S_n(f)$	Receiver input-referred thermal noise PSD, two-sided	A^2/Hz
$n(t)$	Receiver input-referred noise (real, bipolar)	A
$y(t)$	Receiver photocurrent including input-referred noise (real, bipolar)	A
σ_n^2	Noise variance in *n*th subcarrier at memoryless equalizer input	A^2
i_{clip}	Clipping level at A/D input referred to receiver input photocurrent	A
b	Number of A/D quantization bits	bits
$S_{\text{quant}}(f)$	Quantization noise PSD referred to receiver input photocurrent, two-sided	A^2/Hz
SNR_n	SNR of *n*th subcarrier at memoryless equalizer input or output	A^2/A^2

B_n	Achievable bit rate in *n*th subcarrier	bit/s
B_{tot}	Achievable bit rate in all subcarriers	bit/s
Γ	Coding gap ratio ($\Gamma > 1$) depending on FEC code and target error rate	linear units
p_{clip}	Probability of clipping at positive extreme for VCSEL or A/D converter	–

Analysis of Achievable Bit Rate

ACO-OFDM Signal

ACO-OFDM was introduced in [1,2]. In one OFDM symbol period, $0 \le t < T$, the electrical OFDM waveform before clipping is:

$$x(t) = \sum_{n=0,\, n\,\text{odd}}^{N-1} X_n e^{j2\pi f_n t} = 2 \sum_{n=0,\, n\,\text{odd}}^{\frac{N}{2}-1} \text{Re}\left(X_n e^{j2\pi f_n t}\right). \tag{1}$$

This waveform is real because of the Hermitean symmetry condition $X_{N-n} = X_n^*$. Only the odd-indexed subcarriers are modulated, for reasons to be explained shortly. The spectrum of $x(t)$ is shown in Fig. 1. The electrical power of $x(t)$ is:

$$\sigma^2 = E\left(|x(t)|^2\right) = 2 \sum_{n=0,\, n\,\text{odd}}^{\frac{N}{2}-1} E\left(|X_n|^2\right) = 2 \sum_{n=0,\, n\,\text{odd}}^{\frac{N}{2}-1} P_n \,. \tag{2}$$

where the electrical power of the *n*th subcarrier is $P_n = E\left(|X_n|^2\right)$. Assuming the number of subcarriers is sufficiently large, by the Central Limit Theorem, $x(t)$ is Gaussian-distributed with zero mean and variance σ^2.

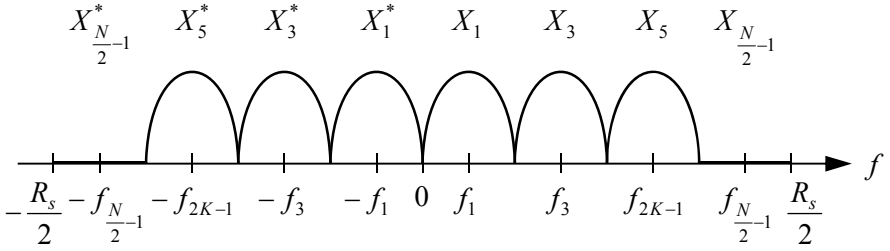

Fig. 1. Schematic spectrum of an ACO-OFDM signal with FFT size N = 16 and K = 3 modulated positive frequency subcarriers, corresponding to an oversampling rate r_{os} = 4/3, illustrating its Hermitean symmetry. Only the modulated odd-indexed subcarriers are shown. For clarity, a single peak at each odd-indexed subcarrier represents a multi-peaked sinc function. Intermodulation products at the even-indexed subcarriers, which result from clipping, are not shown.

After clipping at zero amplitude, the electrical OFDM waveform is:

$$x_+(t) = \begin{cases} x(t) & x(t) \ge 0 \\ 0 & x(t) < 0 \end{cases}. \tag{3}$$

As shown in [1], clipping causes intermodulation distortion only on the even-indexed subcarriers, and the odd-indexed subcarriers are scaled in amplitude by a factor of 1/2. Considering only the odd-indexed subcarriers, the clipped electrical OFDM waveform is:

$$x_+(t) = \sum_{n=0,\, n\,\text{odd}}^{N-1} \frac{1}{2} X_n e^{j2\pi f_n t} = \sum_{n=0,\, n\,\text{odd}}^{\frac{N}{2}-1} \text{Re}\left(X_n e^{j2\pi f_n t}\right). \tag{4}$$

The electrical power of $x_+(t)$ is half that of $x(t)$, i.e., $E\left(\left|x_+(t)\right|^2\right) = \sigma^2/2$. As shown in [1], the average amplitude of $x_+(t)$ is

$$E\left(\left|x_+(t)\right|\right) = \frac{\sigma}{\sqrt{2\pi}}. \tag{5}$$

An ACO-OFDM signal is an optical intensity waveform proportional to $x_+(t)$, so its average optical power is proportional to $\sigma/\sqrt{2\pi}$.

Transmission Link

Figure 2 shows an optical transmission link using ACO-OFDM. The electrical ACO-OFDM waveform $x_+(t)$ drives a VCSEL having d.c. slope efficiency κ and intensity modulation transfer function $H_l(f)$ normalized to unity at d.c., yielding a modulated optical signal $P(t)$. The modulated optical signal $P(t)$ passes through a MMF having intensity modulation transfer function $H_f(f)$. The received optical signal is detected by a photodetector of responsivity *R*, assumed to have an ideal frequency response, yielding a noiseless photocurrent $i(t)$. An input-referred noise $n(t)$ is added, yielding a receiver output $y(t)$. The signal processing for OFDM is described in [1,2,3].

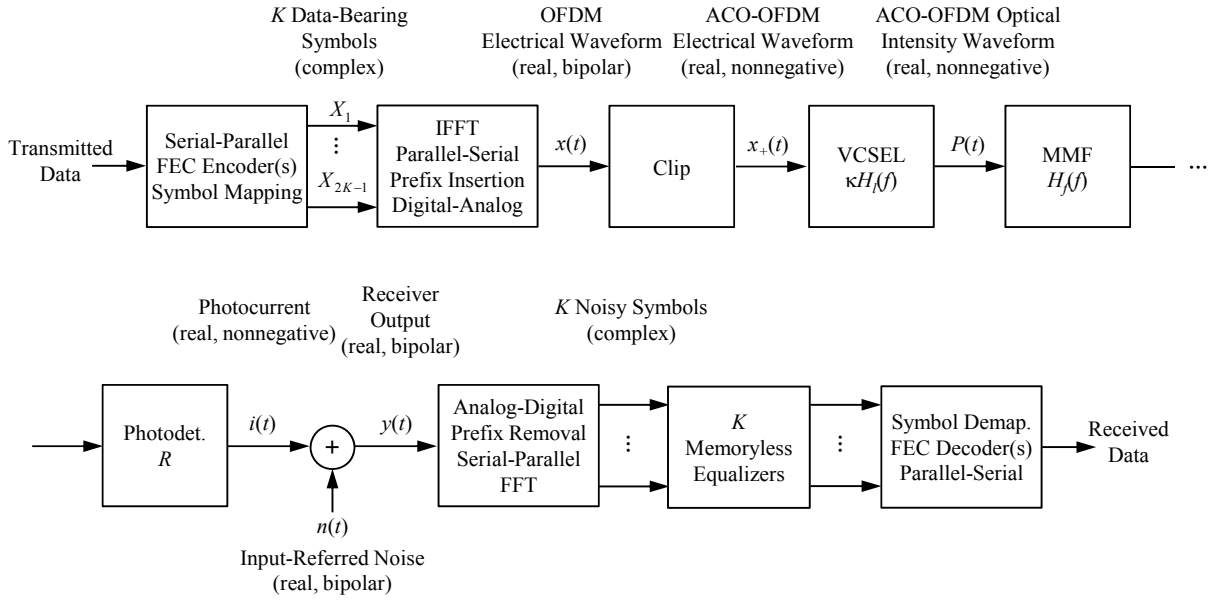

Fig. 2. Block diagram of ACO-OFDM link.

VCSEL Electrical Power Dissipation

Assuming the VCSEL has a series resistance R_l, the electrical power dissipation in the VCSEL is:

$$P_{\text{diss}} = R_l E\left(\left|x_+(t)\right|^2\right) = \frac{R_l \sigma^2}{2} = R_l \sum_{n=0,\, n\,\text{odd}}^{\frac{N}{2}-1} P_n \,, \tag{6}$$

where we have used (2).

VCSEL Average and Peak Optical Power

The VCSEL average output power is computed making reference to Fig. 3(a). The waveform $x(t)$ is first clipped to yield $x_+(t)$, which is then filtered by the VCSEL response $\kappa H_l(f)$, which describes lowpass filtering by electrode parasitics and the intrinsic relaxation oscillation-limited response, followed by electrical-to-optical conversion. If the VCSEL had an ideal transfer function $H_l(f) = 1$, then we would have $P(t) = \kappa x_+(t)$, and the average optical power would be:

$$P_{\text{avg}} = \kappa E\left(\left|x_+(t)\right|\right) = \frac{\kappa\sigma}{\sqrt{2\pi}} = \left(\frac{\kappa^2}{\pi} \sum_{n=0,\, n\,\text{odd}}^{\frac{N}{2}-1} P_n\right)^{\frac{1}{2}}, \tag{7}$$

where we have used (2) and (5). Including a nonideal VCSEL transfer function $H_l(f)$, it becomes difficult to compute P_{avg} analytically. Hence, we rearrange Fig. 3(a) to obtain Fig. 3(b). This corresponds to first filtering $x(t)$ to obtain $x'(t) = \kappa \sum_{n=0,\, n\,\text{odd}}^{\text{N-1}} H_l(f_n) X_n e^{j2\pi f_n t}$, then clipping $x'(t)$ to obtain an optical intensity waveform $P'(t)$. Since $x'(t)$ has a variance

$$\sigma'^2 = E\left(\left|x'(t)\right|^2\right) = 2\kappa^2 \sum_{n=0,\, n\,\text{odd}}^{\frac{N}{2}-1} \left|H_l(f_n)\right|^2 P_n \,, \tag{8}$$

using (5), we obtain an estimate of the average optical power at the VCSEL output:

$$P_{\text{avg}} \approx E\left(\left|x'(t)\right|\right) = \frac{\kappa\sigma'}{\sqrt{2\pi}} = \left(\frac{\kappa^2}{\pi} \sum_{n=0,\, n\,\text{odd}}^{\frac{N}{2}-1} \left|H_l(f_n)\right|^2 P_n\right)^{\frac{1}{2}}. \tag{9}$$

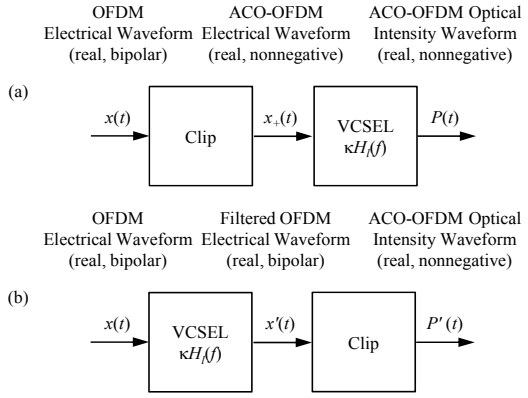

Fig. 3. Rearrangement of portion of Fig. 2 for computing the average optical power P_{avg} and the peak optical power P_{clip} at the VCSEL output.

If the VCSEL had no peak output power limitation, as N is increased, the peak value of the intensity waveform $P(t)$ would become very large, and would become infinite if $x(t)$ were Gaussian-distributed.

In practice, the VCSEL would perform soft or hard clipping of the intensity waveform. To simplify the analysis, we assume that the OFDM encoder, VCSEL driver or VCSEL performs hard clipping at a level corresponding to an output power P_{clip}. We assume P_{clip} is set high enough that clipping occurs infrequently with probability p_{clip}, which is low enough that any resulting errors are tolerable or can be corrected by the FEC coding. Given a tolerable value of the clipping probability p_{clip}, we can compute the required clipping power level P_{clip} making reference to Fig 4. We assume that $x'(t)$ is Gaussian-distributed with variance σ'^2 given by (8). This allows us to obtain:

$$P_{\text{clip}} = \sigma' Q^{-1}\left(\frac{p_{\text{clip}}}{2}\right), \tag{10}$$

where $Q^{-1}(\ )$ is the inverse of the Gaussian Q function.

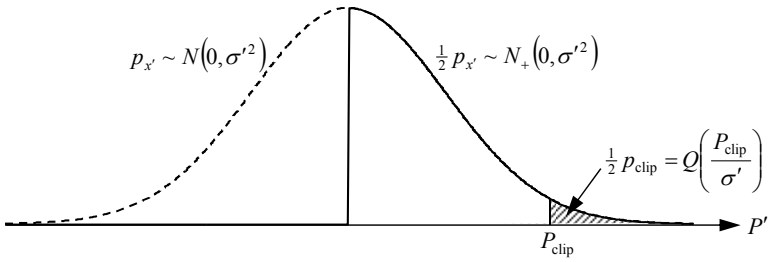

Fig. 4. Illustrating computation of optical intensity clipping level P_{clip}.

Quantization Noise

In the system shown in Fig. 2, quantization effects will limit the achievable performance at the high values of SNR that are required to achieve very high bit rates over a channel of limited bandwidth. The dominant effect is expected to be quantization noise in the A/D converter at the receiver, which we analyze here. We neglect quantization effects in the D/A converter at the transmitter, as well as finite-word-length effects in the DSP units at the transmitter and receiver. For simplicity, we neglect the additive noise $n(t)$ and assume the A/D is quantizing the noiseless photocurrent $i(t)$. We also neglect the gain of the tranimpedance amplifier and any additional amplifiers after the photodetectors, which does not affect the result. Assuming the A/D converter has a limited resolution, the impact of quantization noise is minimized by clipping $i(t)$ at some large positive value [4], which we denote by i_{clip}. We can define a fictitious bipolar photocurrent signal $i'(t)$ which, when clipped at zero amplitude, yields $i(t)$, i.e., $i(t) = i'_+(t)$. Recall that $x'(t)$ is defined in Fig. 3(b) and has a variance σ'^2 given by (9). We observe that $i'(t)$ corresponds to filtering $x'(t)$ by the MMF transfer function $H_f(f)$ and scaling it by the photodetector responsivity R. Hence, $i'(t)$ has a variance:

$$\sigma_{i'}^2 = 2\kappa^2 R^2 \sum_{n=0,\, n\,\text{odd}}^{\frac{N}{2}-1} \left|H_l(f_n)\right|^2 \left|H_f(f_n)\right|^2 P_n \ . \tag{11}$$

We can compute the relationship between the A/D clipping level i_{clip} and the corresponding clipping probability p_{clip} by making reference to Fig 5. Given a tolerable clipping probability p_{clip}, the required clipping level is:

$$i_{\text{clip}} = \sigma_{i'} Q^{-1}\left(\frac{p_{\text{clip}}}{2}\right). \tag{12}$$

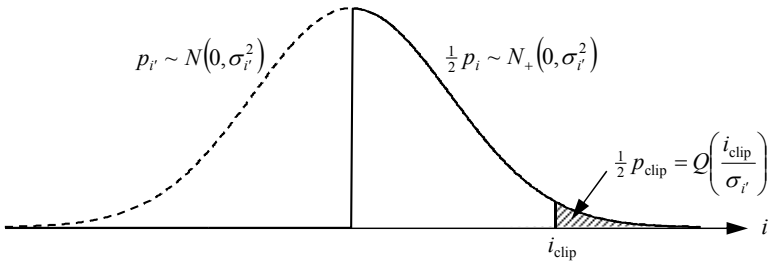

Fig. 5. Illustrating computation of quantizer clipping level i_{clip}.

Assume the A/D converter quantizes signals over the range $[0, i_{\text{clip}}]$ to b bits. Then referred to the A/D input or the photodetector output current $i(t)$, the quantization noise is uniformly distributed over an interval $\left[-\frac{1}{2}2^{-b} i_{\text{clip}}, \frac{1}{2}2^{-b} i_{\text{clip}}\right]$ and has a variance [4]:

$$\sigma_{\text{quant}}^2 = \frac{2^{-2b} i_{\text{clip}}^2}{12}. \tag{13}$$

This is equivalent to a noise having a power spectrum

$$S_{\text{quant}}(f) = \begin{cases} \dfrac{\sigma_{\text{quant}}^2}{R_s} & |f| \le \dfrac{R_s}{2} \\ 0 & |f| > \dfrac{R_s}{2} \end{cases}, \tag{14}$$

which is shown in Fig. 6. Note that in the receiver of Fig. 2, after taking the FFT, the quantization noise should become approximately Gaussian-distributed.

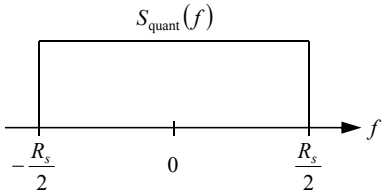

Fig. 6. Equivalent power spectrum of input-referred quantization noise.

Signal-to-Noise Ratio

We can compute the SNR using the analysis given in [3]. At the input to the memoryless equalizer shown in Fig. 2, the nth odd-indexed subcarrier has a signal component with complex amplitude:

$$\frac{\kappa R}{2} H_l(f_n) H_f(f_n) X_n, \tag{15}$$

and with an energy:

$$\frac{\kappa^2 R^2}{4} |H_l(f_n)|^2 |H_f(f_n)|^2 P_n. \tag{16}$$

Recall that the factor of 1/2 in (15) and the factor of 1/4 in (16) arise from clipping at zero amplitude [1,2]. The noise component has a variance:

$$\frac{N+L-1}{N}\Delta f\left[S_n(f_n)+S_{\text{quant}}(f_n)\right], \tag{17}$$

where the factor $(N+L-1)/N$ represents the SNR penalty caused by transmission of a cyclic prefix [3]. Hence, the SNR in the *n*th odd-indexed subcarrier is:

$$SNR_n = \frac{\frac{\kappa^2 R^2}{4}\left|H_l(f_n)\right|^2\left|H_f(f_n)\right|^2 P_n}{\frac{N+L-1}{N}\Delta f\left[S_n(f_n)+S_{\text{quant}}(f_n)\right]}. \tag{18}$$

Achievable Bit Rate

We assume a coding gap ratio Γ depending on the FEC coding scheme and the target error probability, as in [5]. Γ can range from less than 3 dB for a near-capacity-achieving code (such as an LDPC or Turbo code) to as large as 12.2 dB for uncoded QAM modulation at a target symbol-error probability of 10^{-12}. In the *n*th subcarrier, the achievable bit rate is:

$$B_n = \Delta f \log_2\left(1+\frac{SNR_n}{\Gamma}\right). \tag{19}$$

In (19), we see that Γ is an SNR penalty describing how far the FEC scheme lies from the ideal channel capacity at the target error probability. In order to facilitate computing the optimal allocation of power among the modulated subcarriers, we define a noise-to-gain ratio for the *n*th subcarrier:

$$NGR_n = \frac{\frac{N+L-1}{N}\Delta f\left[S_n(f_n)+S_{\text{quant}}(f_n)\right]}{\frac{\kappa^2 R^2}{4}\left|H_l(f_n)\right|^2\left|H_f(f_n)\right|^2}. \tag{20}$$

This allows us to express the achievable bit rate in the *n*th subcarrier as:

$$B_n = \Delta f \log_2\left(1+\frac{P_n}{\Gamma NGR_n}\right). \tag{21}$$

Including all modulated subcarriers, the total achievable bit rate is:

$$B_{\text{tot}} = \sum_{n=0,\, n\,\text{odd}}^{\frac{N}{2}-1} B_n . \tag{22}$$

Optimal Power Allocation

We want to compute the optimal power allocation $\left\{P_n, 0 \le n \le \frac{N}{2}-1, n \text{ odd}\right\}$, which maximizes the total bit rate (22), subject to a constraint on the average optical power (9). In the typical case, (22) depends on the power allocation only through the P_n appearing in the numerator of the term in the logarithm in (21). In this problem, the NGR_n appearing in the denominator also depends on the power allocation, since the power allocation affects the A/D clipping level i_{clip}, which affects the quantization noise variance. Instead of trying to include this dependence in the optimization, we will assume that we know the clipping level prior to optimizing the power allocation. After computing an optimized power

allocation, we will compute the resulting clipping level. If this doesn't match the level assumed in optimizing the power allocation, we will adjust it and repeat the optimization until they match. In practice, this process converges in just a singe iteration.

Optimization of the power allocation is a non-standard problem, because the average power (9) depends not only on the subcarrier powers $\left\{P_n, 0 \le n \le \frac{N}{2}-1, n \text{ odd}\right\}$, but also depends on values of the VCSEL transfer function $\left\{\left|H_l(f_n)\right|^2, 0 \le n \le \frac{N}{2}-1, n \text{ odd}\right\}$.

If we ignore the latter dependence, optimization of the power allocation corresponds to a standard problem [3]. We refer to the solution as *power allocation 1*:

$$P_n = \begin{cases} A - \Gamma NGR_n & \Gamma NGR_n \le A \\ 0 & \Gamma NGR_n > A \end{cases}, \; 0 \le n \le \tfrac{N}{2}-1, \; n \text{ odd} \;, \tag{23}$$

where the constant A is chosen to satisfy a constraint on the average power (9).

If we include the latter dependence and derive the optimal power allocation from scratch, we obtain *power allocation 2*:

$$P_n = \begin{cases} \dfrac{A}{\left|H_l(f_n)\right|^2} - \Gamma NGR_n & \Gamma NGR_n \le \dfrac{A}{\left|H_l(f_n)\right|^2} \\ 0 & \Gamma NGR_n > \dfrac{A}{\left|H_l(f_n)\right|^2} \end{cases}, \; 0 \le n \le \tfrac{N}{2}-1, \; n \text{ odd} \;, \tag{24}$$

where A is chosen to satisfy a constraint on the average power (9). Power allocation 2 allocates higher powers to subcarriers at higher frequencies to compensate for lowpass filtering in the VCSEL. This achieves slightly higher bit rates for the same average optical output power, but requires much higher electrical drive powers, which raises concerns about VCSEL heating and decreased VCSEL lifetime.

Numerical Results

All simulations assume the following:

- VCSEL and MMF properties shown in Fig. 7. Figure 7(a) shows the VCSEL response, which assumes a cutoff frequency (at –3 dB) of 20 GHz and a damping constant of 0.95. Figure 7(b) shows the MMF response, which assumes a cutoff frequency of 25 GHz and a loss of 3 dB.

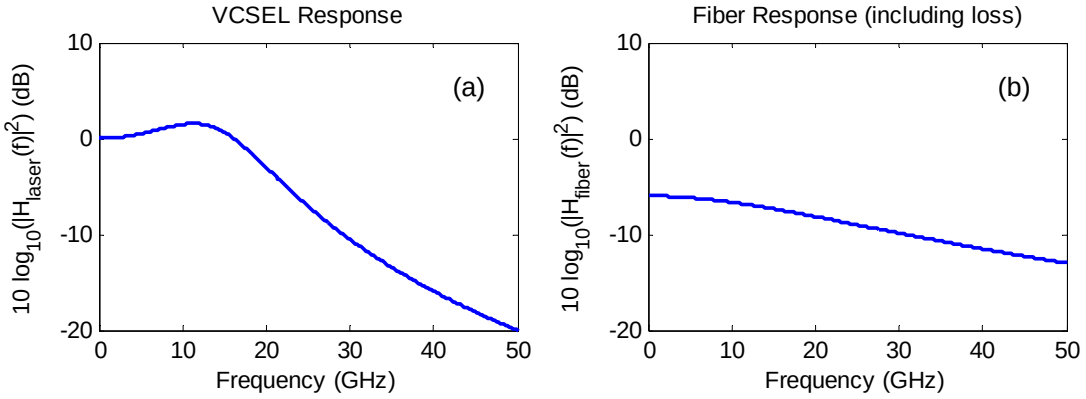

Fig. 7. (a) Electrical magnitude responses of a VCSEL (f_{VCSEL} = 20 GHz, z = 0.95), not including slope efficiency, normalized to 0 dB at d.c. (b) Electrical magnitude response of an MMF (f_{MMF} = 25 GHz, optical loss = 3 dB).

- VCSEL average output power P_{avg} = 1 mW. While output powers as high as 3 mW may be considered eye-safe, the lower output power is chosen because of concerns about peak power limitations in the VCSEL.
- Photodetector with quantum efficiency $\eta = 0.9$. Transimpedance preamplifier with feedback resistance R_F = 100 Ω and noise figure F_n = 6 dB. The total input-referred receiver noise has a two-sided power spectral density $S_n = 2kTF_n / R_F$ [6].
- Sampling rate R_s = 64 GHz, as in long-haul 100 Gbit/s transmission systems. Effective numbers of quantization bits b = 5 and 6 are considered.
- FFT length N = 64, corresponding to $N/4$ = 16 used positive-frequency subcarriers. With a cyclic prefix length L = 5, the cyclic prefix penalty is 0.26 dB, which is modest. Further increases in N can reduce the penalty slightly, but will increase signal processing complexity. Perhaps more importantly, at these relatively small values of N, approximating an OFDM signal as Gaussian-distributed is slightly pessimistic, and there may be room for slight performance improvements (in terms of quantization noise and VCSEL peak output power) compared to the current estimates if N is kept small.

Three major factors are varied in the simulations: (1) FEC coding gap Γ and clipping probability p_{clip}, (2) number of quantization bits B, and (3) power allocation.

Each simulation shows: (a) b = 5 bits, power allocation 1, (b) b = 5 bits, power allocation 2, (c) b = 6 bits, power allocation 1 and (d) b = 6 bits, power allocation 2.

Figure 8 shows results for no coding, where we assume Γ = 12.2 dB for a target error probability of 10^{-12}, and assume a tolerable clipping probability $p_{clip} = 10^{-12}$.

Figure 9 shows results for moderate coding, where we assume Γ = 6.6 dB and assume $p_{clip} = 10^{-5}$. This kind of performance is achieved by FEC schemes widely used in long-haul systems. They are typically based on products or concatenation of Reed Solomon or BCH codes, and typically use non-iterative hard-decision decoding.

Figure 10 shows results for strong coding, where we assume Γ = 3.0 dB and assume $p_{clip} = 10^{-3}$. This kind of performance is achieved by FEC schemes proposed for next-generation long-haul systems, which are typically based on Turbo or LDPC codes with iterative soft-decision decoding. These FEC schemes require much larger chip areas and much higher power consumption, and have much higher latency, than the moderate coding schemes.

Increasing the strength of the coding has the obvious benefit of making the system more tolerant to additive Gaussian noise, which increases the achievable bit rate. It may offer the additional benefit of allowing the system more tolerant to clipping, which may allow operation with a VCSEL having lower peak output power with a smaller A/D quantization range, which reduces the impact of quantization noise. It seems unrealistic to assume strong coding, so moderate coding (Fig. 9) is probably the most realistic case to consider.

Increasing the number of quantization bits from 5 to 6 has the obvious benefit of reducing quantization noise and increasing achievable bit rates.

Power allocation 1 has the benefit of minimizing VCSEL power dissipation, which is under or close to 10 mW in all cases considered. It has the obvious drawback of achieving lower bit rates. A less obvious drawback is that the SNRs and the bits per symbol vary substantially across the subcarriers, which implies that different modulation orders and code rates must be used on different subcarriers in order to achieve bit rates close to those estimated here.

Power allocation 2 has the drawback of requiring much higher VCSEL power consumption, which is close to 25mW in all cases considered. It has the obvious benefit of achieving higher bit rates. A less

obvious benefit is that the SNRs and the bits per symbol are less variable across the subcarriers, which implies that it may be possible to achiever bit rates close to those estimated here by using less disparate modulation orders and code rates on the different subcarriers.

References

1. J. Armstrong and A. J. Lowery, "Power-efficient optical OFDM", *Electronics Letters*, vol. 42, no. 6, pp. 370-372, March 16, 2006.
2. J. Armstrong, B. J. C. Schmidt, D. Kalra, H. A. Suraweera and A. J. Lowery, "Performance of Asymmetrically Clipped Optical OFDM in AWGN for an Intensity Modulated Direct Detection System", *Proceedings of IEEE Global Communications Conference*, 2006.
3. J. M. Kahn, *Lecture Notes for EE 379: Digital Communication*, "Multicarrier Modulation", Stanford University, Winter 2012-13.
4. A. V. Oppenheim and R. W. Schafer*, Discrete-Time Signal Processing, Third Edition*, Prentice-Hall, 2010.
5. D. J. F. Barros and J. M. Kahn, "Comparison of Orthogonal Frequency-Division Multiplexing and On-Off Keying in Direct-Detection Multimode Fiber Links", *Journal of Lightwave Technol*ogy, vol. 29, no. 15, pp. 2299-2309, August 1, 2011.
6. J. M. Kahn, *Lecture Notes for EE 247: Introduction to Optical Fiber Communications*, "Receiver Noises and Signal-to-Noise Ratio Calculations", Stanford University, Autumn 2013-14.

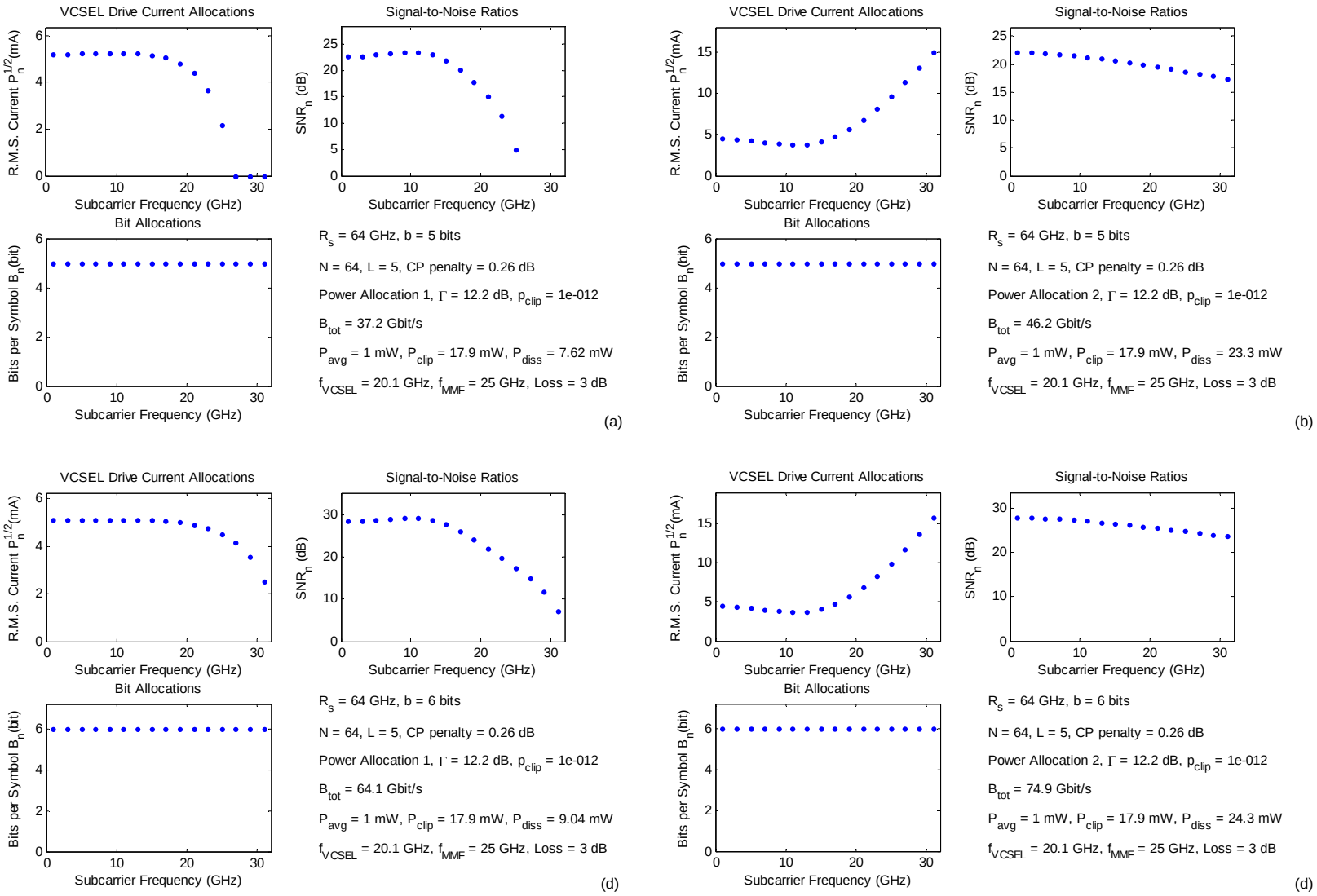

Fig. 8. No coding: Γ = 12.2 dB, $p_{\text{clip}} = 10^{-12}$: (a) 5 bits, power allocation 1, (b) 5 bits, power allocation 2, (c) 6 bits, power allocation 1, (d) 6 bits, power allocation 2.

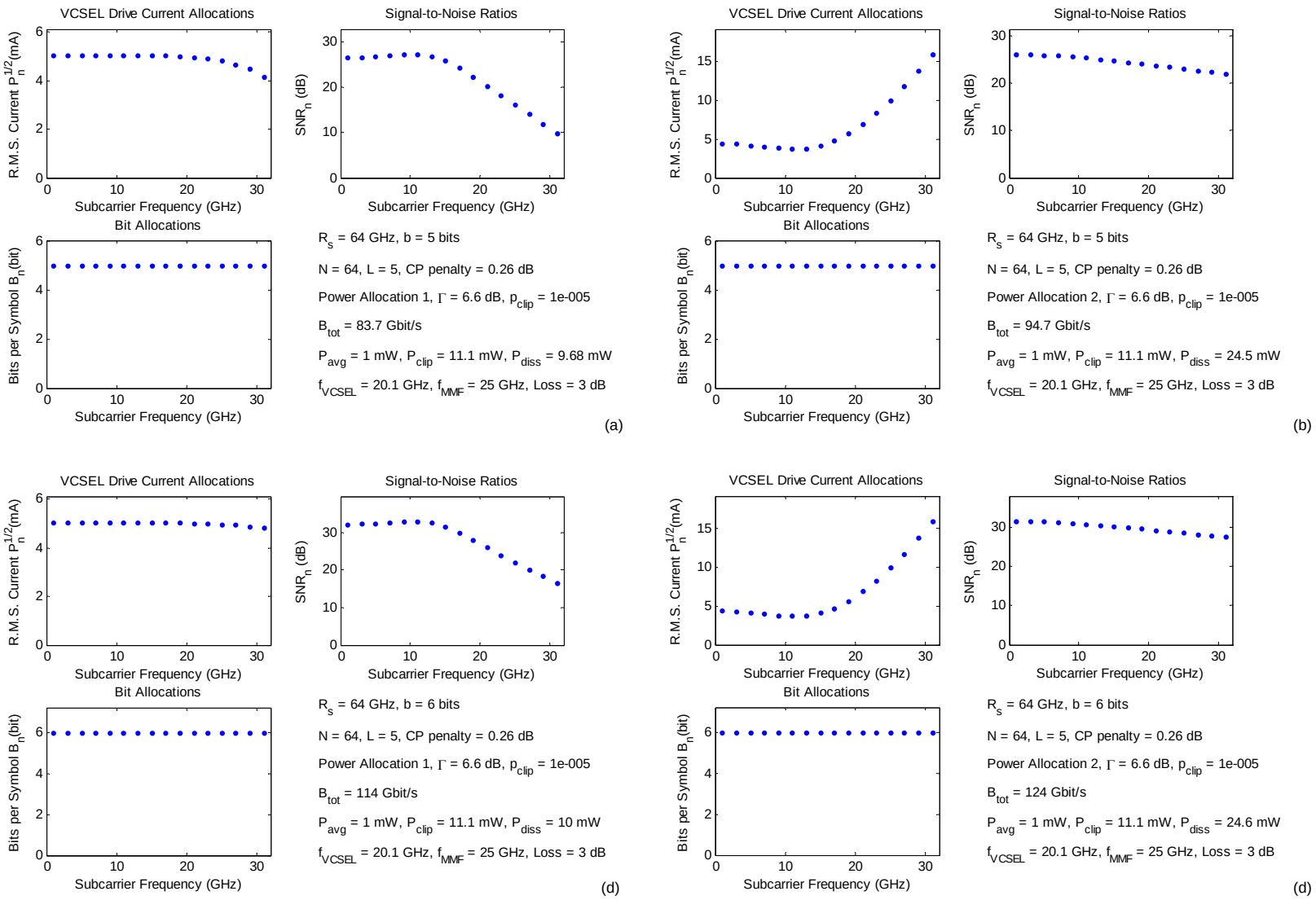

Fig. 9. Moderate coding: $\Gamma = 6.6$ dB, $p_{\text{clip}} = 10^{-5}$: (a) 5 bits, power allocation 1, (b) 5 bits, power allocation 2, (c) 6 bits, power allocation 1, (d) 6 bits, power allocation 2.

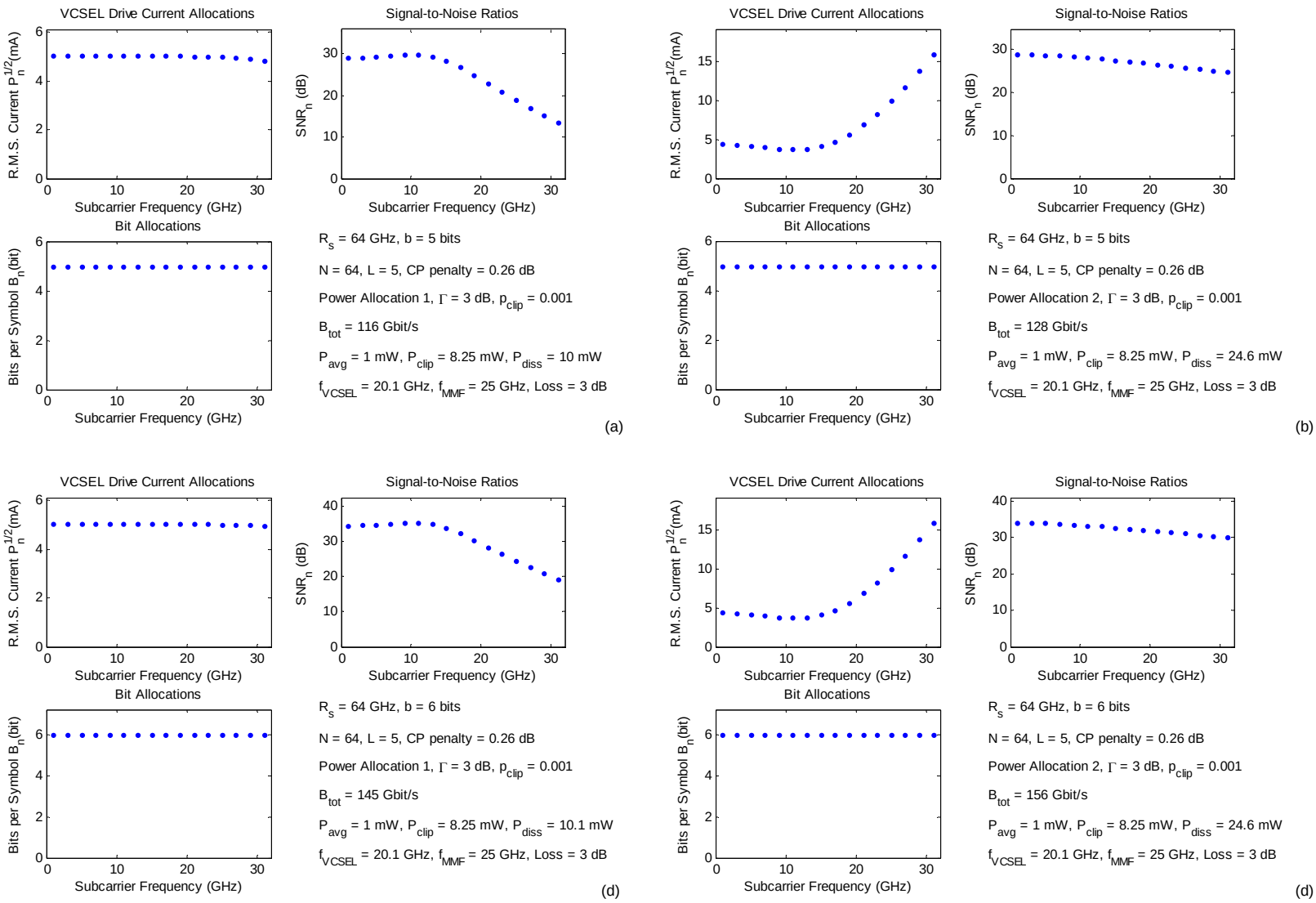

Fig. 10. Strong coding: $\Gamma = 3.0$ dB, $p_{\text{clip}} = 10^{-3}$: (a) 5 bits, power allocation 1, (b) 5 bits, power allocation 2, (c) 6 bits, power allocation 1, (d) 6 bits, power allocation 2.